Transmission and absorption in a waveguide with a metamaterial cavity

Aasim Ullah Jan[1, a)] and R. Porter[2, b]

[1] *Department of Mathematics, COMSATS Institute of Information Technology, Islamabad, Pakistan.*[c]

[2] *School of Mathematics, University Walk, University of Bristol, Bristol, BS8 1TW, UK.*

The reflection and transmission of acoustic waves along a waveguide of uniform width by a metamaterial cavity is considered. The metamaterial is comprised of a closely-spaced array of micro-channels separated by thin plates between which the field may be damped. Exact equations governing the field in the microstructured metamaterial cavity are replaced by an effective field using homogenisation approach. This allows a solution to be formulated in terms of an integral equation across the interface between the metamaterial cavity and the waveguide. Attention focusses on the resonant and damping effects of a metamaterial cavity of tapered height where rainbow trapping phenomena are encountered. It is shown that near-perfect broadbanded absorption of the incoming wave energy can be achieved.

[a)] aasim.math@gmail.com

[b)] richard.porter@bristol.ac.uk

[c] Permanent address: Department of Mathematics and Statistics, Bacha Khan University, Charsadda, Pakistan.

I. INTRODUCTION

The Helmholtz resonator is a classical device used for suppressing transmission of waves along waveguides by enhancing reflection and/or absorption of wave energy[1]. The resonator is usually comprised of a chamber with a narrow neck which connects to the waveguide. The geometry of the Helmholtz resonator determines its resonant frequencies and its interaction with propagating waveguide modes becomes significant close to these frequencies[2]. For example, when damping is absent total reflection can occur and, with visco-thermal losses accounted for, it is possible to absorb up to half of the incident wave energy close to resonance[3]. Perfect absoprtion can be achieved by two resonators[4,5] and multiple resonators, tuned to different frequencies, extend these effects over multiple frequencies[6], having a close connection to a phenomenon labelled "rainbow trapping" in Physics[7].

In undamped periodic arrays of scatterers, stop bands are defined as the ranges of frequencies over which unattenuated wave propagation is prohibited within the array; these generally depend on scattering geometry and spacing. Rainbow trapping occurs when arrays are designed with a slow modulation of geometry and/or spacing along their length[8–10] and waves of different frequencies encounter stop bands at different positions along the array. At the edges of stop bands the group velocity is zero and a field of high intensity is locally trapped. Thus, a modulated array acts to block wave transmission over a broad range of wave frequencies. When damping is added, broadbanded absorption of wave energy can be induced[6,11].

Rainbow trapping can be achieved by passive structures or micro-resonators in 2D or 3D[12,13]. One such device is to use a comb-like grating consisting of an array of grooves of tapered length or width which act as micro-resonators[8–10,14].

In this paper we consider a two-dimensional waveguide with a cavity attached to one wall. The cavity possesses a microstructure consisting of multiple equally-spaced narrow channels separated by thin parallel plates extending perpendicular to the waveguide. Each micro-channel acts as a Helmholtz resonator whose fundamental resonant frequency depends on its length. By arranging the micro-channels to extend over a range of lengths in a linearly-tapered array we construct a broadbanded resonant cavity. The assumption of narrowness of the micro-channels implies that in the physical setting of acoustics viscous losses will be important and should be included in the governing equations. Within this paper we model these losses by adding a linear damping[3],[15] which manifests itself as a complex-valued wavenumber within the cavity.

The solution to the problem of discrete micro-channels is hard to solve by exact analytical methods and it is typical to use Finite Element Method simulations[8–10,14], or asymptotic approximations[16]. Instead, here we take advantage of the contrast in lengthscales between the microstructure and the other lengthscales in the problem and use a homogenisation approach to replace the microstructured cavity by an effective medium/continuum. This particular approximation has been shown to work well when compared to exact mathematical description of the array in a related problem[17].

Within the framework of linearised acoustics the mathematical solution to the boundary-value problem is treated semi-analytically, by employing Fourier transforms within the waveguide and matching to an exact description of the effective wave field within the cavity. The matching gives rise to an integral equation for an unknown function across the join between waveguide and cavity. Application of a standard Galerkin approximation results in a linear system of equations which is straightforward to compute – details are contained in Section 2 of the paper. Section 3 considers expressions for the damping coefficient, a measure of the proportion of wave power absorbed by the cavity. Section 4 contains a range of results and extended discussion of various features of the solution which arise and conclusions follow in Section 5.

II. DESCRIPTION OF THE PROBLEM

In terms of two-dimensional Cartesian coordinates (x, y) a compressible fluid fills a long uniform waveguide with sound-hard walls along $y = 0$, $-\infty < x < \infty$ and $y = a$, $|x| > c$. A cavity attaches to the waveguide along a finite length of one wall $\{|x| < c,\ y = a\}$. Inside this cavity the compressible fluid fills narrow channels between a closely-spaced cascade of thin parallel plates aligned with the y-axis. The length of each of the channels can vary as a function of x as illustrated in Fig. 1.

Within the waveguide, $\Re\{\psi(x, y)\mathrm{e}^{-\mathrm{i}\omega t}\}$ represents time-harmonic variations of the pressure field where the complex-valued function $\psi(x, y)$ satisfies

$$(\nabla^2 + k^2)\psi = 0, \qquad -\infty < x < \infty,\ 0 < y < a. \tag{1}$$

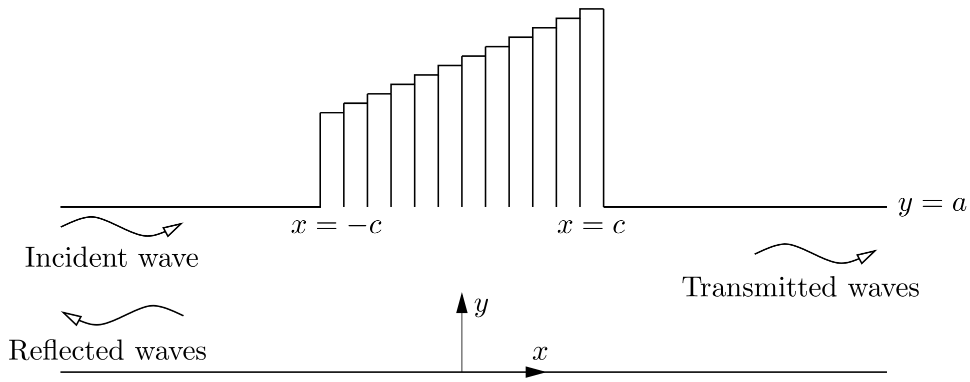

FIG. 1. Definition sketch of the waveguide and plate-array metamaterial cavity.

where $k = \omega/c_s$ where c_s is the wave speed in the waveguide. The walls of the waveguide are sound-hard so

$$\psi_y(x,0) = 0, \qquad \text{and} \qquad \psi_y(x,a) = 0, \qquad \text{for } |x| > c. \tag{2}$$

A wave of unit amplitude is incident from $x = -\infty$ and is partially reflected and partially transmitted due to the effect of the cavity. Separation of variables applied to (1) with (2) in $|x| > c$ determines that

$$\psi(x,y) \sim \mathrm{e}^{\mathrm{i}kx} + \sum_{n=0}^{N} R_n \mathrm{e}^{-\mathrm{i}\alpha_n x} \cos(n\pi y/a), \qquad x \to -\infty \tag{3}$$

and

$$\psi(x,y) \sim \sum_{n=0}^{N} T_n \mathrm{e}^{\mathrm{i}\alpha_n x} \cos(n\pi y/a), \qquad x \to \infty \tag{4}$$

where R_n, T_n are reflection and transmission coefficients, to be found, and the higher-order wavenumbers are defined by the real quantities

$$\alpha_n = \sqrt{k^2 - (n\pi/a)^2}, \qquad n = 0, 1, \ldots, N \tag{5}$$

and $N = \lfloor ka/\pi \rfloor$ is the integer part of ka/π.

Within the cavity, the closely-spaced array of plates has the effect of restricting the propagation of waves to the y-direction and the equation governing the fluid/plate microstructure is represented by

$$(\partial_{yy} + \mu^2)\psi = 0 \tag{6}$$

in $y > a$ for $|x| < c$. A formal derivation of (6) can be made by rescaling the x-coordinate within micro-channels width d where $\epsilon = kd \ll 1$. Equating orders of magnitude in ϵ uses the local lateral boundary conditions on the micro-channel walls en route to the derivation of (6); see[16]. In (6), $\mu \in \mathbb{C}$ replaces k to allow viscous damping effects within the cavity due to the narrowness of the micro-channels, and is defined (see[15] §2.7, for example) by

$$\mu = k + \mathrm{i}\sqrt{k}\sigma, \qquad \sigma = (\nu/2c_s)^{1/2}/(2d) \tag{7}$$

where ν is the kinematic viscosity of the fluid and a small adjustment to the real component of the wavenumber has been neglected.

We remark that the current problem has an analogue in electromagnetic setting for TM-polarised waves in two-dimensional waveguide with perfectly-electric conducting surfaces in which μ represents the effect of a dielectric[18,19]. In accordance with the use of a continuum model (6) to describe the microstructure of the array, the terraced upper boundary of the metamaterial cavity illustrated in Fig. 1 is represented by the continuous line $y = b + mx$ (such that $b \pm mc > a$); on this boundary we impose

$$\psi_y = 0. \tag{8}$$

Solutions of (6) with (8) are given by

$$\psi(x, y) = u(x)\frac{\cos\mu(b + mx - y)}{\mu\sin\mu(b + mx - a)} \tag{9}$$

in terms of the unknown function $u(x) = \psi_y(x,a)$ for $|x| < c$.

Within the waveguide, solutions are sought using Fourier transforms. Thus we define

$$\Psi(l,y) = \int_{-\infty}^{\infty} \left(\psi(x,y) - \mathrm{e}^{\mathrm{i}kx}\right) \mathrm{e}^{-\mathrm{i}lx}\, dx \tag{10}$$

to be the Fourier transform of the scattered part of the field and l is the Fourier transform variable. The inverse is

$$\psi(x,y) = \mathrm{e}^{\mathrm{i}kx} + \frac{1}{2\pi}\int_{-\infty}^{\infty} \Psi(l,y)\mathrm{e}^{\mathrm{i}lx}\, dl \tag{11}$$

in which the contour of integration will be defined to satisfy the radiation condition. That is the contribution to $\psi(x,y)$ as $x \to \pm\infty$ from the integral must defined outgoing waves.

Taking the Fourier transform of (1) gives

$$\Psi''(l,y) - \gamma^2\Psi(l,y) = 0, \qquad 0 < y < a \tag{12}$$

where $\gamma^2 = l^2 - k^2$, whilst the Fourier transform of (2) gives $\Psi'(l,0) = 0$ and

$$\Psi'(l,a) = \int_{-\infty}^{\infty} \frac{\partial}{\partial y}\left(\psi(x,y) - \mathrm{e}^{\mathrm{i}kx}\right)_{y=a} \mathrm{e}^{-\mathrm{i}lx}\, dx = U(l) \equiv \int_{-c}^{c} u(x)\mathrm{e}^{-\mathrm{i}lx}\, dx \tag{13}$$

using (2). Thus, the transform function can be written

$$\Psi(l,y) = \frac{U(l)\cosh\gamma y}{\gamma\sinh\gamma a} \tag{14}$$

and using (11) we have

$$\psi(x,y) = \mathrm{e}^{\mathrm{i}kx} + \frac{1}{2\pi}\int_{-\infty}^{\infty} \frac{U(l)\cosh\gamma y}{\gamma\sinh\gamma a}\mathrm{e}^{\mathrm{i}lx}\, dl. \tag{15}$$

It is evident from (15) that there are poles on the axis of integration at $l = \pm\alpha_n$ for $n = 0,\ldots,N$ and these relate to propagating modes at $x \to \infty$. In order that energy is outgoing, the contour is chosen to pass below the poles $l = \alpha_n$ on the positive real l-axis and above the poles $l = -\alpha_n$ on the negative real l-axis. This definition means that as $x \to \infty$,

$$\psi(x, y) \sim \mathrm{e}^{\mathrm{i}kx} + \sum_{n=0}^{N} \frac{\mathrm{i}\epsilon_n(-1)^n U(\alpha_n)}{2\alpha_n a} \mathrm{e}^{\mathrm{i}\alpha_n x} \cos(n\pi y/a) \tag{16}$$

where $\epsilon_0 = 1$, $\epsilon_n = 2$ for $n \geq 1$, an expression found by deforming the contour of integration into the upper-half plane and evaluating contributions from the poles along $l = \alpha_n$. Similarly, we find that as $x \to -\infty$

$$\psi(x, y) \sim \mathrm{e}^{\mathrm{i}kx} + \sum_{n=0}^{N} \frac{\mathrm{i}\epsilon_n(-1)^n U(-\alpha_n)}{2\alpha_n a} \mathrm{e}^{-\mathrm{i}\alpha_n x} \cos(n\pi y/a) \tag{17}$$

found by deforming the contour of integration into the lower-half plane and evaluating contributions from poles at $l = -\alpha_n$.

Comparing with (3), (4) we find that

$$R_n = \frac{\mathrm{i}\epsilon_n(-1)^n U(-\alpha_n)}{2\alpha_n a}, \qquad n = 0, 1, \dots, N \tag{18}$$

and

$$T_n = \delta_{n0} + \frac{\mathrm{i}\epsilon_n(-1)^n U(\alpha_n)}{2\alpha_n a}, \qquad n = 0, 1, \dots, N. \tag{19}$$

The formulation is completed by matching the two representations of $\psi(x, y)$, (9) and (15) across the common boundary $y = a$, $|x| < c$. Thus

$$\frac{\cot \mu(b - a + mx)}{\mu} u(x) - \frac{1}{2\pi} \int_{-\infty}^{\infty} \frac{\coth \gamma a}{\gamma} \mathrm{e}^{\mathrm{i}lx} \int_{-c}^{c} u(x')\mathrm{e}^{-\mathrm{i}lx'}\, dx'\, dl = \mathrm{e}^{\mathrm{i}kx} \tag{20}$$

for $|x| < c$ represents an integral equation for $u(x)$.

A numerical solution of this equation will be sought by expanding $u(x)$ using a finite complex Fourier series over $-c < x < c$. I.e. we write

$$u(x) \approx \sum_{p=-P}^{P} c_p u_p(x/c), \qquad \text{where } u_p(t) = (-1)^p \mathrm{e}^{\mathrm{i}p\pi t}/c \tag{21}$$

in which c_p are coefficients to be determined and the value of P will be chosen to ensure the numerical solution is sufficiently converged – this is discussed further in the results section. Substituting (21) into (20) and then multiplying by the conjugate $u_q^*(x/c)$, $q = -P, \dots, P$ and integrating over $-c < x < c$ gives the algebraic system of equations

$$\sum_{p=-P}^{P} (L_{pq} - M_{pq})\, c_p = F_q(kc), \qquad q = -P, \dots, P \tag{22}$$

for the unknown coefficients c_p where

$$L_{pq} = \frac{(-1)^{p+q}}{2\mu c^2} \int_{-c}^{c} \mathrm{e}^{\mathrm{i}\pi(p-q)x/c} \cot \mu(b - a + mx)\, dx \tag{23}$$

and

$$M_{pq} = \frac{1}{\pi} \int_{-\infty}^{\infty} \frac{\coth \gamma a}{\gamma} F_p(lc) F_q(lc)\, dl \tag{24}$$

with

$$F_p(lc) = \frac{1}{2} \int_{-c}^{c} u_p(x/c) \mathrm{e}^{-\mathrm{i}lx}\, dx = \frac{\sin(lc)}{lc - p\pi}. \tag{25}$$

Note that if $m = 0$, $L_{pq} = \delta_{pq} \cot[\mu(b - a)]/(\mu c)$. Work is also required to arrange M_{pq} into a computable form and these details are contained in the Appendix.

Using (21) in (17), (18) with (13) gives

$$R_n = \frac{\mathrm{i}\epsilon_n(-1)^n}{\alpha_n a} \sum_{p=-P}^{P} c_p F_p(-\alpha_n c), \qquad n = 0, \dots, N \tag{26}$$

and

$$T_n = \delta_{n0} + \frac{\mathrm{i}\epsilon_n(-1)^n}{\alpha_n a} \sum_{p=-P}^{P} c_p F_p(\alpha_n c), \qquad n = 0, \dots, N. \tag{27}$$

III. DAMPING

The time-averaged flux of energy crossing a boundary S with unit normal $\hat{\mathbf{n}}$ is calculated, for any pressure field $p(x, y)$ satisfying (1), from

$$\frac{\omega\rho}{2}\Im\left\{-\int_S p(\hat{\mathbf{n}}\cdot\nabla p^*)\,ds\right\}. \tag{28}$$

where ρ is the fluid density, ds is the arclength along S and the asterisk denotes complex conjugate. When $p(x, y) = \mathrm{e}^{\mathrm{i}kx}$ and the boundary, S, is the interval $0 < y < a$ for a constant x, the quantity above equates to $\frac{1}{2}\omega\rho a$; this is the power in the incident wave of unit amplitude travelling along the waveguide defined in §2.

In the scattering problem considered in the previous section, we can evaluate the outgoing energy flux by application of (28) to the function $p(x, y) \equiv \psi(x, y) - \mathrm{e}^{\mathrm{i}kx}$ for $x \to -\infty$ as given by (3) and by application of $p(x, y) = \psi(x, y)$ as $x \to \infty$ as in (4).

The mean energy absorption ratio – or *damping coefficient* – is defined by the mean incoming power minus the total mean outgoing power normalised by the mean incoming power. For the problem considered in §2 this is calculated to be

$$\eta = 1 - \sum_{n=0}^{N}\frac{\alpha_n}{\epsilon_n}\left(|R_n|^2 + |T_n|^2\right). \tag{29}$$

I.e. $\eta = 0$ is non-absorbing and $\eta = 1$ represents total absorption of incident wave energy.

An independent calculation of η can be obtained by measuring the mean rate of energy loss across the boundary $y = a$, $-c < x < c$ between the cavity and the waveguide using (28). Once normalised with respect to the power of the incoming wave of unit amplitude, this gives

$$\eta = \frac{1}{a}\Im\left\{-\int_{-c}^{c}\psi(x, a)\psi_y^*(x, a)\,dx\right\}. \tag{30}$$

When used with the definition (9) this gives

$$\eta = \frac{1}{a}\Im\left\{-\int_{-c}^{c}|u(x)|^2\frac{\cot\mu(b+mx-a)}{\mu}\,dx\right\}. \tag{31}$$

In terms of the results of the numerical scheme the above is expressed as

$$\eta \approx -\frac{2c}{a}\Im\left\{\sum_{p=-P}^{P}\sum_{q=-P}^{P}c_p c_q^* L_{pq}\right\}. \tag{32}$$

When $m = 0$ the simplification to L_{pq} reduces this to expression to

$$\eta \approx -\frac{2c}{a}\Im\left\{\cot[\mu(b-a)]/(\mu c)\right\}\sum_{p=-P}^{P}|c_p|^2. \tag{33}$$

Either (29) or (32)/(33) for $m = 0$ can be used to calculate the damping coefficient. Numerically, we find agreement between the two expressions to machine precision in computed results (indeed, it can be proved with some effort that one does imply the other) and thus serves only as a check on the implementation of the method, not an indicator of the accuracy of the numerical results.

IV. RESULTS

The focus of our results are $|R_n|$, $|T_n|$, the amplitude of the scattering coefficients and on the damping coefficient η. Numerically these are computed by (26), (27) and (29) or (32) which depend on the solution to the system of equations (22). Approximations result from the truncation to $2P+1$ terms of the system of equations and from the truncation of the infinite integrals. We have conducted exhaustive tests on convergence of the results and conclude that truncating integrals to $l = 400$ and using $P = 5$ gives accuracy to more than four decimal places in all results presented, apart from where special comments apply. For

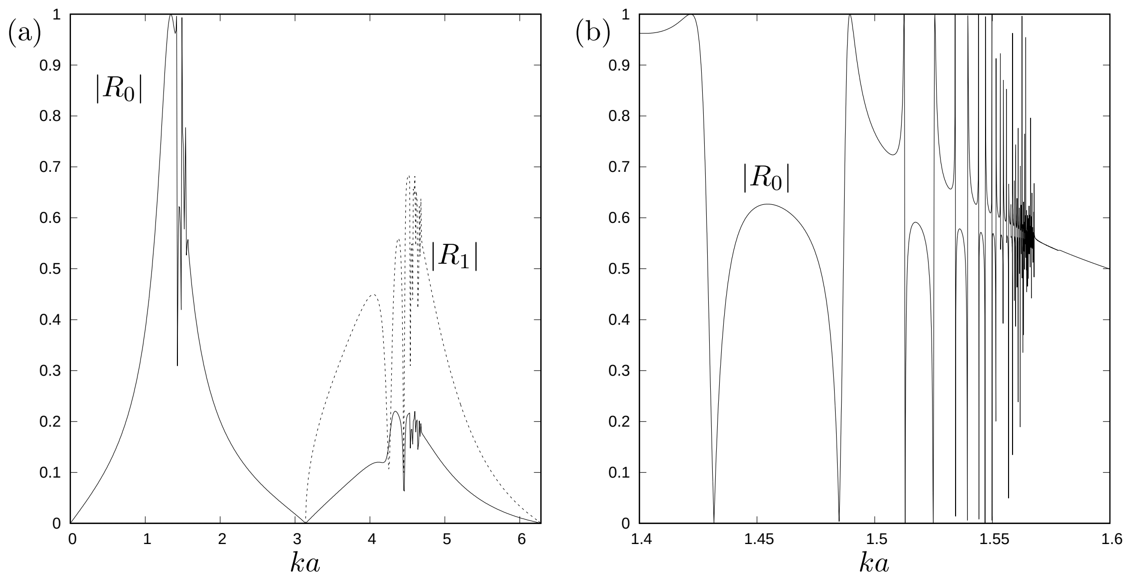

FIG. 2. Variation of reflection coefficients with ka (magnified scale in (b)) for a lossless rectangular metamaterial cavity $b/a = 2$, $c/a = 0.2$, $m = 0$ and $\mu = k$.

many, but not all, cases truncation to $l = 10$ and using $P = 1$ are sufficient; the numerical scheme is generally very quick and efficient to run.

We start by considering $m = 0$ so that the metamaterial cavity is rectangular and $\mu = k$ so that there is no damping. We pick an example which illustrates the effect of this basic cavity by selecting $b/a = 2$, $c/a = 0.2$. Results showing the amplitudes of the reflected and transmitted wave coefficients $|R_n|$, $|T_n|$ are shown, as ka varies, in Fig. 2(a) with Fig. 2(b) focussing on results close to $ka = \frac{1}{2}\pi$. The higher order modes are cut-on at $ka = n\pi$, $n = 1, 2, \ldots$ and thus there are two modes shown in $\pi < ka < 2\pi$. We have displayed only reflected wave amplitudes in order to make the graphs presentable. The behaviour of scattering coefficients is complicated as ka approaches $\frac{1}{2}\pi$ and $\frac{3}{2}\pi$.

These two values have a particular physical significance as they are related to the eigen-solutions to the 1D wave equation in the channels formed by the metamaterial. That is, at these frequencies the channels within the metamaterial cavity support a resonant wave with a node at the opening, $y = a$, and an antinode at the end of the channel, $y = b$. For the rectangular cavity considered in Fig. 2, this resonance condition is the same for all micro-channels: $ka = (q + \frac{1}{2})\pi/(b/a - 1)$, $q = 0, 1, \ldots$. Thus, in the case shown in Fig. 2, where $b/a = 2$, resonance is predicted at $ka = \frac{1}{2}\pi$ and $ka = \frac{3}{2}\pi$.

A higher numerical truncation parameter, P, is required as $ka \to \frac{1}{2}\pi$ to resolve the increasingly oscillatory behaviour of the scattering coefficients, suggesting an increasing frequency in oscillations in the field between the two sidewalls of the cavity. This has been confirmed by numerical results not shown here.

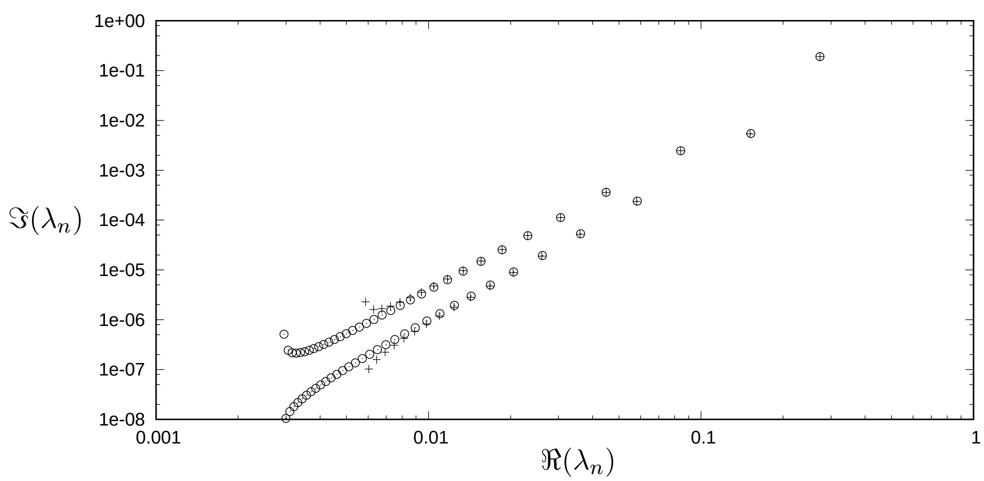

FIG. 3. The eigenvalues of the matrix M with elements M_{pq} for $P = 32$ (circles) and $P = 16$ (crosses) and with $ka = 1.5$, $b/a = 2$, $c/a = 0.2$.

In order to understand the complex behaviour seen in the results we need to understand the integral operator in (20). The operator is non-self-adjoint principally on account of the particular sense in which deformations have been made to the contour of integration to avoid poles in $|l| \leq 1$ located on the real integration axis. A self-adjoint version of the integral operator, in which integration is confined to the real l-axis and with integration across poles are interpreted in the Cauchy principal-value sense, has the property that its eigenvalues, λ_n, are positive and have zero as a limit point (i.e. with $0 < \lambda_{n+1} < \lambda_n$, $\lambda_n \to 0$ as $n \to \infty$)[20]. In this regard an alternative formulation of the problem is possible in which this self-adjoint operator takes the part of the existing non-self-adjoint operator in (20) but happens at the expense of increased algebraic complication elsewhere; the rearrangement of terms give rise to a scattering matrix formulation reliant on the solution of $2N+2$ uncoupled integral equations. However, it is not clear that pursuing such an approach brings any clear advantage or clarity to the problem.

In the numerical method the eigenvalues of the non-self-adjoint integral operator are manifested as eigenvalues of the matrix M (with elements M_{pq} defined by (24)). There are now a finite number of these eigenvalues which are complex but with imaginary parts smaller than their real parts – see Fig. 3. The sequence of eigenvalues formed by taking an increased truncation parameter P tends to zero with positive real and imaginary parts and matches the behaviour anticipated above. When $m = 0$ and $\mu = k$, $b/a = 2$ the matrix elements $L_{pq} = \delta_{pq} \cot(ka)$ from (23) and it is clear from (22) that near resonance arises when the real-valued $\cot(ka)$ passes close to the complex eigenvalues of the matrix M. With reference to Fig. 5 as $ka \to \frac{1}{2}\pi$ from below this happens with increasing frequency and the strength of the near resonance increases; this explains the plot in Fig. 2. Note that the same effect is replicated at higher frequencies – as $ka \to (q + \frac{1}{2})\pi/(b/a - 1)$ for any integer $q = 0, 1, \ldots$ and any value of b/a.

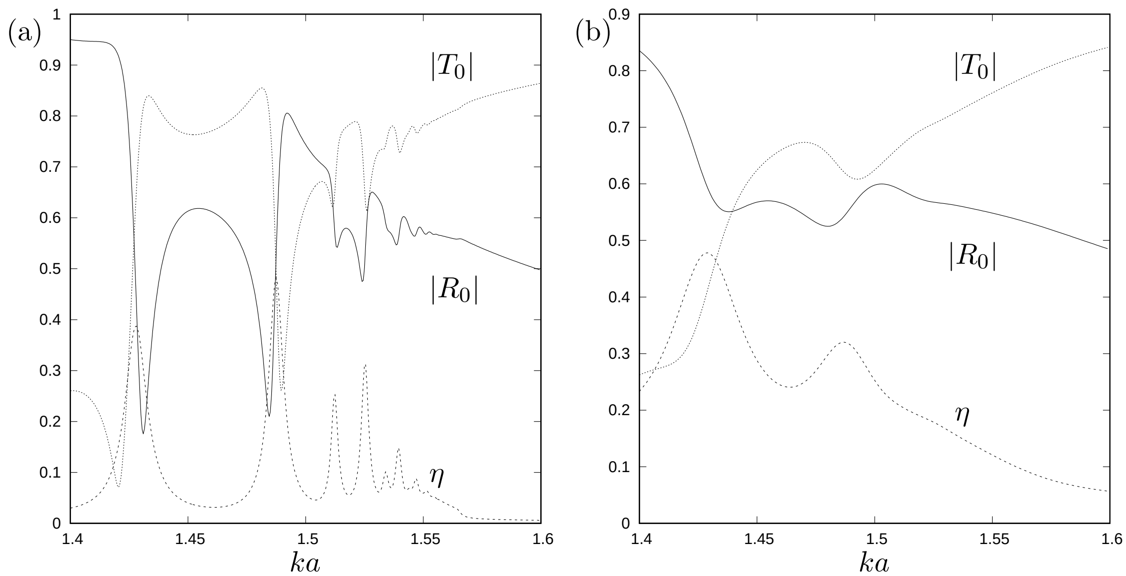

FIG. 4. Variation of scattering and damping coefficients with ka for a rectangular metamaterial cavity $b/a = 2$, $c/a = 0.2$, $m = 0$ and $\mu = k + \mathrm{i}\sigma\sqrt{k}$ with $\sigma = 0.001$ in (a) and $\sigma = 0.01$ in (b).

It is tempting to conclude that there is no solution in Fig. 2 at $ka = \frac{1}{2}\pi$. However for $b/a = 2$, $m = 0$, $ka = \frac{1}{2}\pi$ the solution in the metamaterial cavity satisfies $\psi(x, a) = 0$ for $|x| < c$. Thus, the solution in the waveguide must satisfy $\psi(x, a) = 0$ for $|x| < c$ in addition to (1), (2) and radiation conditions and is therefore decoupled from the solution in the cavity. This waveguide boundary-value problem is well-posed and the solution can be expressed using Fourier transforms by (20) but with the first term absent. The solution, $u(x)$, representing $\psi_y(x, a)$, $|x| < c$, sets the value of $\psi(x, y)$ within metamaterial cavity. On account of the boundary condition across $|x| < c$ being homogenous Dirichlet and (2) for $|x| > c$ being homogeneous Neumann, the solution, $u(x)$, is known to possess inverse square root singularities as $|x| \to c^-$, (e.g.[2]). We have used a modified set of functions

$$u_p(t) = \frac{2\mathrm{e}^{-\mathrm{i}p\pi/2} T_p(t)}{\pi\sqrt{1 - t^2}}, \tag{34}$$

where $T_n(t)$ are Chebychev functions, in place of those defined in (22)[2] which results in $F_p(lc) = J_p(lc)$ replacing (25). The revised numerical scheme has been used to compute accurate and rapidly-convergent solutions for the specific case relating to $ka = \frac{1}{2}\pi$ in Fig. 2.

Computation of results for the problem with parameters used in Fig. 2 evaluated at exactly $ka = \frac{1}{2}\pi$ returns values for $|R_0|$ of 0.551615 ($P = 8$), 0.551301 ($P = 16$), 0.55115 ($P = 32$) and 0.55113 ($P = 64$). With (34) we find $|R_0| = 0.55105$ to five significant figures with a truncation parameter of $P = 1$.

In Figs. 4(a,b) we consider the effect on the results shown in Fig. 2 of adding small (but increasing) amounts of damping. Thus we retain the geometrical parameters $m = 0$ and $b/a = 2$, $c/a = 0.2$, but take $\mu = k + 0.001\mathrm{i}\sqrt{k}$ and $\mu = k + 0.01\mathrm{i}\sqrt{k}$ in the two plots. In Figs. 4(a,b) we add the transmission coefficient, $|T_0|$, and the damping coefficient, η. A small amount of damping smooths out the rapid fluctuations in scattering coefficients.

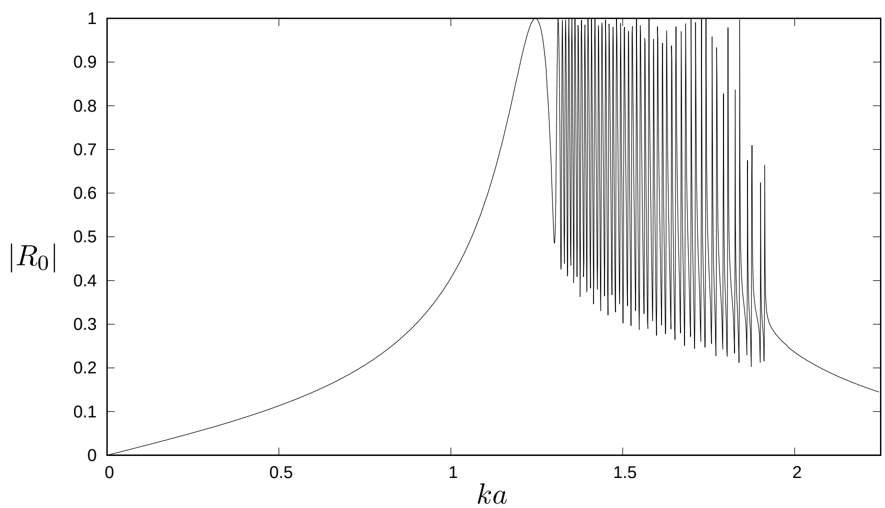

FIG. 5. Variation of $|R_0|$ with ka for a lossless ($\mu = k$) tapered metamaterial cavity $b/a = 2$, $c/a = 0.2$, $m = 1$.

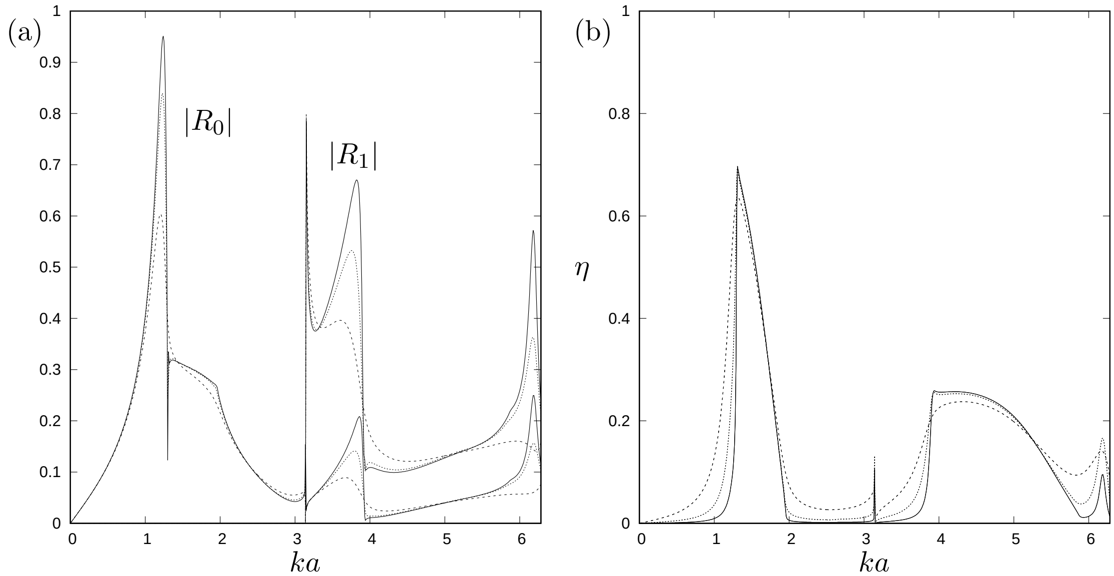

FIG. 6. Variation of (a) scattering and (b) damping coefficients with ka for a lossy tapered metamaterial cavity $b/a = 2$, $c/a = 0.2$, $m = 1$: $\mu = k + 0.0025\mathrm{i}\sqrt{k}$ (solid), $\mu = k + 0.01\mathrm{i}\sqrt{k}$ (dashed), $\mu = k + 0.04\mathrm{i}\sqrt{k}$ (dotted).

We stick with $b/a = 2$ and $c/a = 0.2$ in Figs. 5, 6 where the effect of changing cavity taper, m, is considered. We have shown results for $m = 1$, so that the cavity taper is angled at 45°. In Fig. 5 results are given for a lossless cavity ($\mu = k$). For these parameters there is a continuous range ($1.309 < ka < 1.963$) of resonant frequencies embedded within the metamaterial cavity over which $|R_0|$ oscillates rapidly. The number of oscillations is set by the truncation parameter – $P = 24$ in Fig. 5. When P is halved or doubled the number of oscillations in this range is halved or doubled although the vertical extent of the oscillations forms a robust and well-defined envelope (the resolution of the plot accounts for random variations in the vertical). Thus, it appears that the numerical solution does not converge as $P \to \infty$ and this single issue has been at the centre of most of the work performed on this paper.

Various alternative approaches have been explored to shed light on this. One approach has been to change the numerical approximation scheme. This has included using collocation methods and different basis functions. We have also reformulated the integral equation (20) replacing $u(x) \equiv \phi_y(x, a)$ with $\phi(x, a)$ as the unknown and have used the fact that $\phi(x_*, a) = 0$ to construct a basis where x_* is a solution of $\tan(\mu(b - a + mx_*)) = 0$ and the location of the resonant channel in the metamaterial cavity. By taking this approach we have attempted to remove potential issues with singularities or discontinuities associated with derivatives. Every attempt had resulted in the same outcome, namely non-convergent oscillations whose frequency are tied to the numerical scheme. We note that similar results have been observed in related studies[11]. Finally, an approximation has been made to the current problem which involves replacing the continuum model for the cavity by a finite number of discrete narrow channels, using matched asymptotic expansions to determine overall scattering. The formulation and results are described in a supplementary report,[16]. Not only is this approach able to accurately reproduce the qualitative behaviour of the reflection and transmission coefficients seen in Fig. 5, but it indicates that there are as many zeros of transmission as there are micro-channels in the cavity. Even the envelope of oscillations suggested by Fig. 5 is captured accurately. Thus the oscillations increase as the number of finite channels increase (so that their width decreases in proportion) and we are led to the conclusion that a converged solution to the undamped continuum metamaterial cavity does not exist.

The addition of damping regularises the convergence. In Figs. 6(a,b) we show the reflected wave coefficients and the damping coefficient, η, for the same parameters as in Fig. 5 but with $\mu = k + 0.04\mathrm{i}\sqrt{k}$, $\mu = k + 0.01\mathrm{i}\sqrt{k}$ and $\mu = k + 0.0025\mathrm{i}\sqrt{k}$. The curves are produced with truncation parameters $P = 16$, $P = 32$ and $P = 128$, respectively. It can be seen that as the imaginary part of μ tends to zero, the results converge (although the numerical scheme has to work harder to achieve this) but *not* to a solution for zero damping. In fact, $\eta \to 0$, as the damping parameter tends to zero in all non-resonant intervals of ka. Over intervals of ka where there is resonance (e.g. $1.309 < ka < 1.963$, $3.927 < ka < 5.890$ in Fig. 6) in the metamaterial cavity the damping coefficient η converges to non-zero values and forms a well-defined curve.

We now turn our attention to the potential practical application of this device which is to act as an acoustic damper. In Fig. 7 we have plotted the damping coefficient, η, and the scattering coefficients for a tapered array with $b/a = 2$, $m = 0.25$, $c/a = 4$ and $\mu = k + 0.05\mathrm{i}\sqrt{k}$. Thus, the horizontal extent of the cavity is 8 times the waveguide width, the longest micro-channel is twice the waveguide width and the cavity tapers to micro-channels of zero length. This configuration means there is resonance in the cavity for all $ka > \frac{1}{4}\pi$ and we see that damping is close to 100% for a broad range of values of ka extending from $\frac{1}{4}\pi$ dropping slowly as ka increases beyond π. As already noted in relation to Fig. 6, the shape of the damping coefficent curve is quite robust to changes in the damping parameter.

To some extent, the shape and size of the metamaterial cavity does not affect the high absorption demonstrated in Fig. 7. By way of example, in Fig. 8 we have extended the depth of the cavity by setting $b/a = 3$, retaining $c/a = 4$ using $m = 0.5$ to taper the length of the micro-channels from four times the waveguide width down to zero. Cavity resonances now extend beyond $ka = \frac{1}{8}\pi \approx 0.39$ and in Fig. 8 a damping parameter of $\mu = 1 + 0.1\mathrm{i}$ has

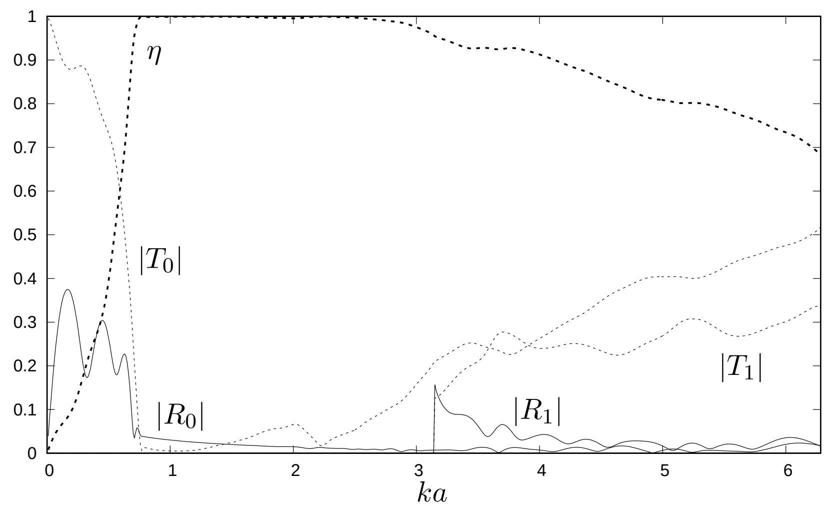

FIG. 7. Variation of η (thick dotted curve) and scattering coefficients with ka for a tapered metamaterial cavity $b/a = 2$, $c/a = 4$, $m = 0.25$ with damping $\mu = k + 0.05\mathrm{i}\sqrt{k}$.

been used to demonstrate once again that high absorption can be achieved (over 98% of the acoustic energy is damped over $0.4 < ka < 2.83$).

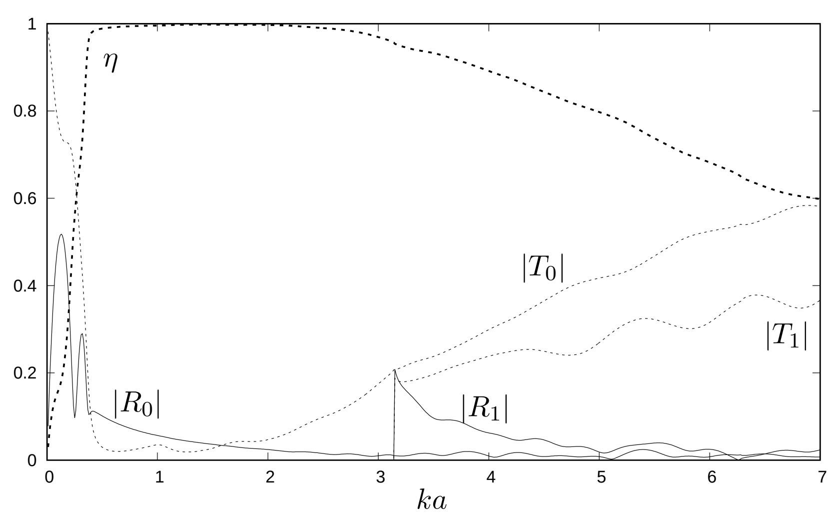

FIG. 8. Variation of η (thick dotted curve) and scattering coefficients with ka for a tapered metamaterial cavity $b/a = 3$, $c/a = 4$, $m = 0.5$ with damping $\mu = k + 0.1\mathrm{i}\sqrt{k}$.

V. CONCLUSIONS

We have presented a simplified mathematical model of a microstructured plate-array metamaterial cavity of a type commonly used in applications of rainbow trapping. The cavity has been attached to the sidewall of a waveguide and its effect on acoustic wave propagation has been considered. The simplified model for the cavity has allowed us to express important features of the problem such as the scattering coefficients and acoustic absorption in terms of the solution of a simple integral equation.

The main purpose of the problem was to consider the efficacy of a tapered metamaterial cavity as a model of a rainbow trapping absorbing device to provide a broadbanded damping of acoustic energy. However, many interesting features of the solution have emerged in the process, relating to resonance in the case where the damping is set to zero. In particular, we have shown that the effective medium/continuum model produces anomalous results when resonance is encountered; in a rectangular metamaterial cavity oscillations in the scattering coefficients increase in frequency without bound as isolated resonant parameters are approached but the limiting case at resonance parameters is well-defined. On the other hand, for a lossless tapered metamaterial cavity possessing a continuous range of resonant parameters the effective medium model appears to be at fault. Numerical results fail to converge, consistent with discrete models of micro-channelled cavities,[16]. A continuum model which includes damping *does* converge numerically for a fixed damping parameter and as this tends to zero results converge, though not to the solution of a zero-damping problem.

Other results have demonstrated that close to 100% of ducted acoustic wave energy can be damped by a tapered array over a broad range of frequencies suggesting that the metamaterial cavity is an extremely effective broadbanded asborber. Work is ongoing on using the continuum model to construct absorbing surfaces using tapered metamaterial cavities.

ACKNOWLEDGMENTS

This work was undertaken during a research visit by the first author to the University of Bristol; funding provided by the Higher Education Commission of Pakistan is gratefully acknowledged.

APPENDIX: COMPUTATION OF INTEGRALS

From (23) we substitute $l \to -l$ for $l < 0$ to write

$$M_{pq} = \frac{2}{\pi} \int_0^\infty \frac{\coth \gamma a}{\gamma} S_{pq}(l)\, dl \tag{A.1}$$

where

$$S_{pq}(l) = \frac{[(lc)^2 + pq\pi^2] \sin^2(lc)}{[(lc)^2 - (p\pi)^2][(lc)^2 - (q\pi)^2]}. \tag{A.2}$$

and the contour of integration has been defined to pass below the poles at $l = \alpha_n$, $n = 0, 1, \ldots, N$. The value of N and hence the number of poles is dependent on ka but there always exists a pole at $l = k$ corresponding to $n = 0$.

Integrals with contours passing below the poles are evaluated as principal-value integrals plus half-residues from the vanishly-small semi-circular indentations of the contour around the poles. The principal-value integral at $l = k$ is dealt with by organising the integral in a form suitable for numerical quadrature with

$$\fint_0^{2k} f(l)\, dl = \int_0^k (f(l) + f(2k - l))\, dl. \tag{A.3}$$

To treat any remaining principal-value evaluations at $l = \alpha_n$ for $n \geq 1$ we write

$$\fint_0^k \frac{f(l)}{g(l)} dl = \int_0^k \left(\frac{f(l)}{g(l)} - \frac{f(\alpha_n)}{(k - \alpha_n) g'(\alpha_n)} \right) dl + \log \left(\frac{k - \alpha_n}{\alpha_n} \right) \frac{f(\alpha_n)}{g'(\alpha_n)} \tag{A.4}$$

where it is assumed that $g(\alpha_n) = 0$ so that the integrand on the right-hand side is now bounded as $l \to \alpha$. With these tricks in place we may write (A.1) as

$$\begin{aligned} M_{pq} = & \frac{2}{\pi} \int_{2k}^{\infty} \frac{\coth(\sqrt{l^2 - k^2} a)}{\sqrt{l^2 - k^2}} S_{pq}(l)\, dl \\ & + \frac{2}{\pi} \int_0^k \left[\frac{\coth(\sqrt{(2k - l)^2 - k^2} a)}{\sqrt{(2k - l)^2 - k^2}} S_{pq}(2k - l) - \frac{\cot(\sqrt{k^2 - l^2} a)}{\sqrt{k^2 - l^2}} S_{pq}(l) \right. \\ & \left. - \sum_{n=1}^{N} \frac{S_{pq}(\alpha_n)}{\alpha_n a (l - \alpha_n)} \right] dl + \frac{\mathrm{i}}{ka} S_{pq}(k) + \frac{2}{\pi} \sum_{n=1}^{N} \frac{(\pi \mathrm{i} + \log(k/\alpha_n - 1))}{\alpha_n a} S_{pq}(\alpha_n) \end{aligned} \tag{A.5}$$

which includes the evaluations from semi-circular intendations below the poles.

The integrand in the real integral over $0 < l < 1$ in (A.5) is smooth and bounded everywhere and can be computed using a standard numerical quadrature. The integrand in the real semi-infinite integral in (A.5) decays like $O(1/l^3)$ and is approximated by truncating the upper limit to $l = 400$.

In the case of $m = 0$, L_{pq} is explicit. For $m \neq 0$ and μ complex the complex-valued integral defined by (23) can be performed by numerical quadrature.

However, when $m \neq 0$ and μ is real special care may be required owing to the fact that the integrand may contain singularities. In such an instance (23) will be defined as principal-value type and we use the same procedure outlined above of subtracting and adding singularities to get

$$L_{pq} = \frac{(-1)^{p+q}}{2\mu c^2} \int_{-c}^{c} \left(\mathrm{e}^{\mathrm{i}\pi(p-q)x/c} \cot \mu(b-a+mx) - \sum_{r=1}^{R} \frac{\mathrm{e}^{\mathrm{i}\pi(p-q)x_r/c}}{\mu m(x-x_r)} \right) dx$$
$$+ \frac{(-1)^{p+q}}{2\mu^2 mc^2} \sum_{r=1}^{R} \mathrm{e}^{\mathrm{i}\pi(p-q)x_r/c} \log\left(\frac{c-x_r}{c+x_r}\right) \tag{A.6}$$

where $x_r \in (-c, c)$ satisfy $\sin \mu(b-a+mx_r) = 0$, $r = 1, \ldots, R$. If no such x_r exists the sums in (A.6) are removed and the original integral in (23) is done directly.

References

[1]Munjal, M.L. *Acoustics of Ducts and Mufflers,* 2nd ed. (John Wiley and Sons, New York, 2014).

[2]Porter, R. and Evans, D.V. "Analysis of the effect of a cavity resonator on acoustic transmission in a waveguide," J. Sound Vib. **408**, 138–153 (2017).

[3]Achilleos, V., Richoux, O. and Pagneux, V. "Coherent perfect absorption induced by the nonlinearity of a Helmholtz resonator," J. Acoust. Soc. Am. **140**, EL94 (2016).

[4]Romero-Garcia, V., Theocharis, G., Richoux, O., Merkel, A., Tournat, V. and Pagneux, V. "Perfect and broadband acoustic absorption by critical coupling," Sci. Rep. **6**, 19519 (2016).

[5]Merkel, A., Theocharis, G., Richoux, O., Romero-Garcia, V. and Pagneux, V. "Control of acoustic absorption in one-dimensional scattering by resonant scatterers," Appl. Phys. Lett. **107**, 244102 (2015).

[6]Jimenez, N., Romero-Garcia, V., Pagneux, V. and Groby, J.-P. "Rainbow-trapping absorbers: Broadband, perfect and asymmetric sound absorption by subwavelength panels for transmission problems," Sci. Rep. **7**, 13595 (2017).

[7]Tsakmakidis, K.L., Boardman, A.D. and Hess, O. " 'Trapped rainbow' storage of light in metamaterials," Nature **450**, 397–401 (2007).

[8]Gan, Q., Ding, Y.J. and Bartoli, F.J. " 'Rainbow' Trapping and Releasing at Telecommunication Wavelengths," Phys. Rev. Lett. **102**, 056801 (2009).

[9]Zhu, J., Chen, Y., Zhu, X., Garcia-Vidal, F.J., Yin, X., Zhang, W. and Zhang, X. "Acoustic rainbow trapping," Sci. Rep. **3**, 1728 (2013).

[10]Montazeri, A.O., Fang, Y., Sarrafi, P., and Kherani, N.P. "Rainbow-trapping by adiabatic tuning of intragroove plasmon coupling," Optics Express **24**(23), 26745 (2016).

[11]Liu, T., Liang, S., Chen, F. and Zhu, J. "Inherent losses induced absorptive acoustic rainbow trapping with a gradient metasurface," J. Appl. Phys. **123**, 091702 (2018).

[12]Kurt, N. and Yilmaz, J.-P. "Rainbow trapping using chirped all-dielectric periodic structures," Appl. Phys. B. **110**(3), 411–417 (2017).

[13]Xiao, Y., Wen, J. and Wen, X. "Sound transmission loss of metamaterial-based thin plates with multiple subwavelength arrays of attached resonators," J. Sound Vib. **331**, 5408–5423 (2012).

[14]Tian, Z. and Yu, L. "Rainbow trapping of ultrasonic guided waves in chirped phononic crystal plates," Sci. Rep. **7**, 40004 (2017).

[15]Lighthill, J. "Waves in Fluids", Cambridge University Press, 1978.

[16]Porter, R. "Scattering in a waveguide with narrow side channels," http://people.maths.bris.ac.uk/~marp/abstracts/narrow-chan.pdf (2018).

[17]Porter, R. "Plate arrays as a water-wave metamaterial," Proc. 33rd Int. Workshop on Water Waves and Floating Bodies, Brest, France. 165–169 (2018).

[18]Hu, H., Ji, D., Zeng, X., Liu, K. & Gan, Q. "Rainbow Trapping in Hyperbolic Metamaterial Waveguide," Sci. Rep. **3**, 1249 (2013).

[19]Cui, Y., Fung, K.H., Xu, J., Ma, H., Jin, Y., He, S. and Fang, N. "Ultrabroadband Light Absorption by a Sawtooth Anisotropic Metamaterial Slab," Nano Lett. **12**, 1443–1447 (2012).

[20]Porter, D. and Stirling, D.S.G. *Integral Equations,* (Cambridge University Press, 1992) p. 107.